Chaos and Broadband Noise in Extrinsic Photoconductors

S. W. Teitsworth and R. M. Westervelt
Department of Physics and Division of Applied Sciences, Harvard University, Cambridge, Massachusetts 02138
(Received 14 September 1984)

A simple model is studied describing low-temperature free-carrier dynamics in extrinsic photoconductors due to capture by impurity atoms and impact ionization. Numerical results are presented which exhibit period doubling, chaotic behavior, and elevated effective noise temperatures. Photoconductor properties necessary for chaotic behavior are discussed.

PACS numbers: 72.70.+m, 72.20.Dp, 72.40.+w

Oscillatory instabilities of a variety of types occur in electrical conduction in semiconductors due to nonlinear effects of high applied electric fields, and have been studied for some time.[1,2] They are typically manifested by the appearance of simply periodic oscillations (e.g., in sample current) as some stress parameter (e.g., electric field) is increased through a threshold value. In recent experiments on Ge[3] and GaAs[4] far-infrared (FIR) photoconductors, and on Ge oscillistors,[5] more complex nonlinear phenomena have been discovered: period doubling, frequency locking, and chaotic oscillation which produces large amounts of broadband noise. While in many cases the physical origin of the simple nonlinear instability is known,[2,5] an understanding of the development from simply periodic to chaotic behavior is only just beginning to emerge. Recent advances in the theory of nonlinear dynamical systems[6,7] can lead to a new understanding of complex instabilities and noise in semiconductor devices.

In this Letter we show that the standard, spatially uniform rate-equation model[2] describing carrier generation and trapping in extrinsic photoconductors can exhibit chaos and the production of broadband noise when excited by periodically modulated external radiation. This is one of the first theoretical demonstrations that nonlinear dynamics can produce intrinsic chaos in semiconductors. We expect that other nonlinear devices, including microwave IMPATT and Gunn diodes,[2] show similar behavior.

The standard rate-equation model describing the time dependence of the hole concentration p and the electric field E for a rectangular device with electrical contacts on opposite faces is

$$\dot{p} = \gamma(a - a_*) + p\kappa(a - a_*) - pra_*, \tag{1}$$

$$\epsilon\dot{E} = J_{\rm ext} - epv, \tag{2}$$

$$p = a_* - d, \tag{3}$$

$$J_{\rm ext}(t) = J_0 + \Delta J \sin(2\pi f_{dr} t). \tag{4}$$

In Eq. (1) a is the total acceptor concentration, a_* is the time-dependent ionized acceptor concentration, γ is the generation rate, and $\kappa(E)$ and $r(E)$ denote the field-dependent impact-ionization and capture rates, respectively. Equation (2) is simply Ampère's law where $\epsilon dE/dt$ is the displacement current and ϵ is the dielectric constant; $J_{\rm ext}$ is the external current density, and $v(E)$ is the field-dependent drift velocity including effects of velocity saturation.[8] In this simple model we assume space-charge neutrality, which is expressed by Eq. (3), where d is the compensating donor concentration. As discussed elsewhere,[9] space charge can have important effects, but these are not essential for the production of chaos. With these assumptions, Eqs. (1)–(3) can be derived from three coupled partial differential equations given in Refs. 3 and 9. In practice the current in extrinsic photoconductors is often determined by modulated FIR illumination which produces a time-dependent component of current $\Delta J \sin(2\pi f_{dr} t)$, modeled by Eq. (4). For the square-wave excitation commonly used the first Fourier component is $\Delta J/J_0 \simeq 1.27$. In previous experiments[3] on ultrapure Ge devices, the FIR illumination was constant, and relaxation-type instabilities associated with space charge trapped near the injecting contact drove the bulk of the semiconductor device which is modeled by Eqs. (1)–(4).

Equations (1) and (2) constitute a damped, driven nonlinear oscillator with dynamical variables $p(t)$ and $E(t)$.[9] Loosely, $E(t)$ is analogous to the position in a mechanical oscillator, while $p(t)$ is analogous to the momentum, $\kappa(E)$ and $r(E)$ play the role of restoring forces,[6,9] and $J_{\rm ext}$ is the drive. Graphs for $\kappa(E)$ and $r(E)$ used in the calculations below are shown in Fig. 1. The numerical forms used for κ and r, which are given in Ref. 9, were derived under the assumption of a drifted Maxwellian velocity distribution for holes with an elevated effective temperature.[9] The capture rate, $r(E)$, is roughly constant for small fields and then drops as E^{-3}, reflecting a decrease in capture cross section

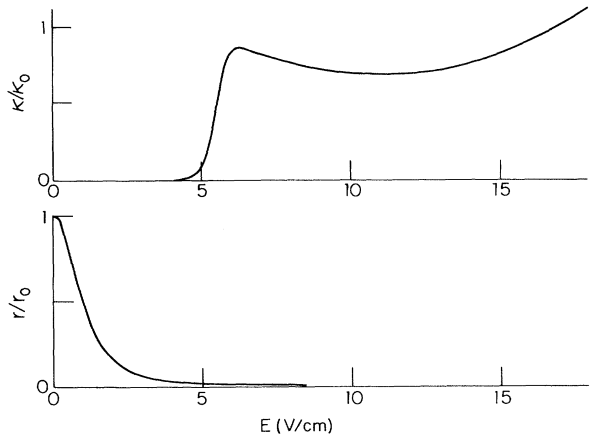

FIG. 1. Plots of $\kappa(E)$ and $r(E)$ with $\kappa_0 = 2\times10^{-6}$ cm^3 sec^{-1} and $r_0 = 1\times10^{-5}$ cm^3 sec^{-1}.

with increasing carrier velocity.[10] The impact ionization rate $\kappa(E)$ is negligible for E much smaller than the breakdown field $E_b \simeq 5$ V/cm because typical carrier kinetic energies are less than the impurity ionization energy B.[3,9] As the field increases through E_b a large number of carriers gain sufficient energy to ionize neutral impurities, resulting in an abrupt increase in $\kappa(E)$. When the average kinetic energy is greater than B, the coefficient $\kappa(E)$ will *decrease* with increasing E because the impact ionization cross section decreases with increasing kinetic energy.[11] Finally, as the hole velocity saturates, $\kappa(E)$ rises again, in part because of additional impurity ionization by emitted optical phonons. A wide variety of differential functional forms for $\kappa(E)$ have been examined; those forms which possess a local maximum produce qualitatively similar results.

All of the numerical results presented here were calculated for parameter values appropriate to ultrapure Ge samples studied in Ref. 3: $a = 10^{11}$ cm^{-3}, $d = 2\times10^{10}$ cm^{-3}, $\gamma = 10^{-4}$ sec^{-1}, $J_0 = 1.3\times10^{-7}$ A/cm^2, $B = 10$ meV, $\epsilon = 16$, and lattice temperature $T = 4.2$ K. For these values and $\kappa(E)$, $r(E)$, and $v(E)$ as previously described, a single stable fixed point is found for Eqs. (1) and (2) with $\Delta J = 0$ at $p_0 \simeq 9.3\times10^4$ cm^{-3}, $E_0 \simeq 4.69$ V/cm. For small perturbations about the fixed point the equations show damped oscillatory response at a frequency $f_0 \simeq 6422$ Hz and with a quality factor $Q \simeq 4.7$.

The response of this system for $f_{dr}/f_0 = 1.45$ is shown in Fig. 2 at four successively larger drive amplitudes ΔJ. This figure shows the phase portrait $p(t)$ vs $E(t)$, the time record of $E(t)$, and the power spectrum $S(f)$ of $E(t)$ as $\Delta J/J_0$ increases from 1.10 to 1.45.[12] Figure 2(a) shows a simply periodic response with $\Delta J/J_0 = 1.10$. The high harmonic content of this nonlinear oscillation is seen in both the phase portrait and time record. Initially $E(t)$ increases which causes $p(t)$ to rise as a result of increased impact ionization. Then $E(t)$ drops as a result of the enhanced dielectric relaxation that results from larger $p(t)$. Period doubling[13] is observed in Fig. 2(b) where the drive strength has been increased to $\Delta J/J_0 = 1.25$. In this case the period doubling and also the chaos depicted below

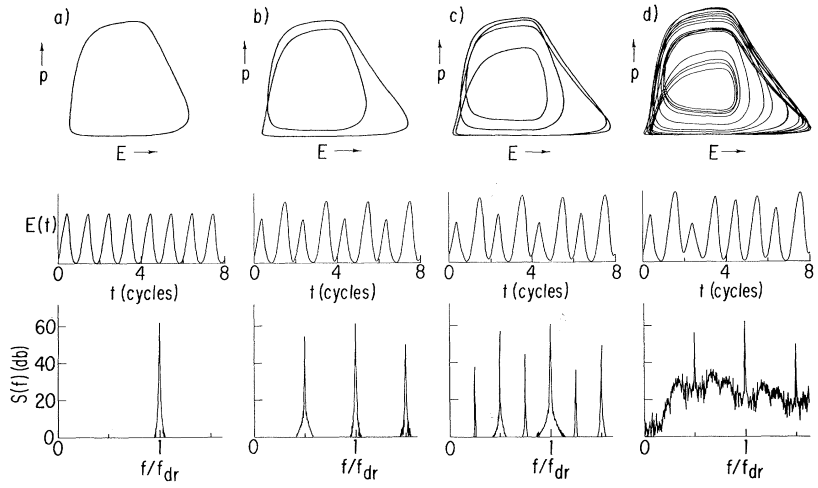

FIG. 2. Phase portrait of $p(t)$ vs $E(t)$, time record of $E(t)$, and power spectrum $S(f)$ of $E(t)$ for driving frequency $f_{dr}/f_0 = 1.45$ and 4 increasing drive amplitudes: (a) $\Delta J/J_0 = 1.10$; (b) $\Delta J/J_0 = 1.25$; (c) $\Delta J/J_0 = 1.35$; and (d) $\Delta J/J_0 = 1.45$. Figures of similar type are plotted with the same scale. For the power spectra 0 dB corresponds to 1×10^{-7} V^2 cm^{-4} Hz^{-1}.

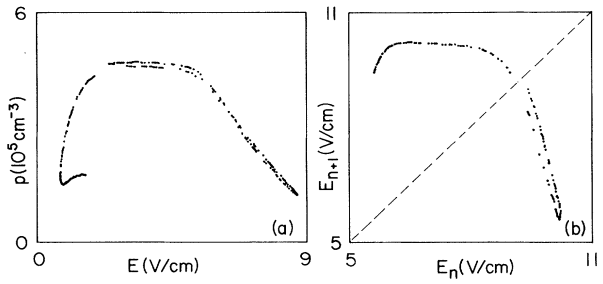

FIG. 3. (a) Poincaré section in p and E, constructed by strobing the phase portrait at constant drive phase. (b) Return map constructed from successive maxima in E. In both (a) and (b) $\Delta J/J_0 = 1.45$ and $f_{dr}/f_0 = 1.45$.

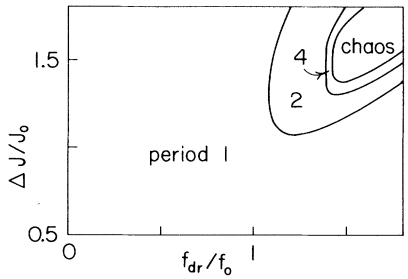

FIG. 4. Phase diagram for the system response at different drive strengths $\Delta J/J_0$ and frequencies f_{dr}/f_0. The region marked 1 denotes simply periodic response, 2 denotes period-2 response, and 4 denotes period-4 and higher response; the chaotic region is also indicated.

are due to the reduction in $\kappa(E)$ beyond its local maximum at $E \simeq 6.3$ V/cm (see Fig. 1). When the trajectory passes into this region, the rate of increase in $p(t)$ is reduced because of less effective impact ionization, producing a phase lag, and the trajectories cross as shown in the phase portrait of Fig. 2(b).

Period 4 is shown in Fig. 2(c) for drive strength $\Delta J/J_0 = 1.35$. Higher-order period doublings including period 8 are observed as the drive is further increased; they accumulate at a critical value $\Delta J/J_0 \simeq 1.39$, at which point the flow becomes chaotic.

Chaos is shown in Fig. 2(d) for $\Delta J/J_0 = 1.45$. As shown in the phase portrait and the time record of $E(t)$ the oscillatory character is not lost, but the motion is no longer periodic. In the power spectrum only the fundamental, the first subharmonic, and their harmonics are still visible. The other peaks have disappeared with a concomitant increase in broadband noise characteristic of the presence of deterministic chaos. The noise level in Fig. 2(d) corresponds to an effective noise temperature of $\sim 10^8$ to 10^9 K for device volumes ~ 1 to 10 mm^3.

A Poincaré section[6] in p and E and a return map constructed from successive maxima of $E(t)$ are shown in Fig. 3. The Poincaré section shows both the beginning of a fold in the lower left-hand corner of Fig. 3(a) and the same fold one cycle later in the right-hand side. This folding and stretching, which is two-banded in this case, provides the mixing of orbits necessary for deterministic chaos. Because the Poincaré section is almost one-dimensional the chaotic flow corresponds approximately to the return map of Fig. 3(b). The map clearly has a coarse structure similar to 1D maps that have been extensively studied,[7,13] although a remnant fold due to the two-dimensional nature of the Poincaré section is also evident.

Figure 4 shows a phase diagram giving the dynamical state of the system for different drive strengths, $\Delta J/J_0$, and drive frequencies, f_{dr}/f_0. For the case $f_{dr}/f_0 = 1.45$ studied above the system eventually returns to nonchaotic behavior for $\Delta J/J_0 \gtrsim 1.7$. The semiconductor oscillator studied here bears a qualitative resemblance to the resistively shunted junction model of a driven Josephson junction which has been extensively studied.[14,15] In contrast to Ref. 14, chaotic behavior here occurs only for values of f_{dr}/f_0 greater than 1 reflecting the stiff nature of the "restoring force." For other parameter values we have observed frequency locking at other ratios including 2:1 and 3:1 followed by period-doubling sequences. Phase diagrams like the one depicted in Fig. 4 are useful in the construction of low-noise semiconductor devices.

One might expect more pronounced chaotic behavior for extrinsic GaAs photoconductors than for Ge. The impurity binding energy $B \sim 6$ meV in GaAs is smaller than for Ge, and a much larger reduction in $\kappa(E)$ is possible before velocity saturation occurs. On the other hand, extrinsic Si photoconductors should be relatively more stable, with respect to this nonlinear mechanism, because the velocity saturates before the carriers heat to the larger binding energies, $B \sim 50$ meV.

We thank E. E. Haller and P. L. Richards for helpful comments. This work was supported in part by the Office of Naval Research and the Joint Services Electronics Program.

[1]B. K. Ridley, Proc. Phys. Soc. London **82**, 954 (1963).
[2]K. Seeger, *Semiconductor Physics* (Springer-Verlag,

New York, 1973).

[3]S. W. Teitsworth, R. M. Westervelt, and E. E. Haller, Phys. Rev. Lett. **51**, 825 (1983).

[4]E. Aoki and K. Yamamoto, Phys. Lett. **98A**, 72 (1983).

[5]G. A. Held, C. D. Jeffries, and E. E. Haller, Phys. Rev. Lett. **52**, 1037 (1984).

[6]J. Guckenheimer and P. Holmes, *Nonlinear Oscillations, Dynamical Systems, and Bifurcations of Vector Fields* (Springer-Verlag, New York, 1983).

[7]E. Ott, Rev. Mod. Phys. **53**, 655 (1981).

[8]L. Reggiani, C. Canali, F. Nava, and G. Ottaviani, Phys. Rev. B **16**, 2781 (1977).

[9]R. M. Westervelt and S. W. Teitsworth, to be published.

[10]M. Lax, Phys. Rev. **119**, 1502 (1960).

[11]N. F. Mott and H. S. W. Massey, *The Theory of Atomic Collisions* (Oxford Univ. Press, New York, 1965), 3rd ed.

[12]The power spectra were obtained by averaging raw power spectra calculated directly from an 8192-point fast-Fourier transform.

[13]M. J. Feigenbaum, J. Stat. Phys. **19**, 25 (1978).

[14]B. A. Huberman, J. P. Crutchfield, and N. A. Packard, Appl. Phys. Lett. **37**, 750 (1980).

[15]D. D'Humieres, M. R. Beasley, B. A. Huberman, and A. Libchaber, Phys. Rev. A **26**, 3483 (1982).